An Ultrahighly Sensitive Electrochemical Biosensor for Cytochrome c with Surface Molecular Imprinting Based on Hybrid Nanomaterials

Qin Wang[1,2], Hao Guo[1], Yuli Wei[3], Rui Xue[3], Baolong Ma[1], Wu Yang[1,]*

[1] College of Chemistry and Chemical Engineering, Key Lab of Bioelectrochemistry and Environmental Analysis of Gansu Province, Northwest Normal University, Lanzhou 730070, PR China
[2] Zhonghao North Paint and Coatings Industry Research Institute Co., Ltd, Lanzhou 730020, PR China
[3] College of Chemistry and Chemical Engineering, Lanzhou City University, Provincical Key Laboratory of Gansu Higher Education for City Environmental Pollution Control, Lanzhou City University, Lanzhou730070, P R China
[*]E-mail: xbsfda123@126.com

A novel ultrahighly sensitive 3D structural electrochemical imprinted biomacromolecular sensor for Cyt c was fabricated based on hybrid polyaniline nanotube/carboxylated multi-walled carbon nanotubes (PANTs-MWCNTs) composites by surface molecular imprinting method on the surface of glassy carbon electrode (GCE). The hybrid nanomaterials can enhance imprinting efficiency. The fabrication and electrochemical behavior of the prepared imprinted biosensor were studied by electrochemical techniques, scanning electron microscopy (SEM) and Fourier transform infrared spectra (FTIR). Under the optimal conditions, the detection of Cyt c with the imprinted sensor exhibited a wide linear range from 1.0×10^{-14} to 1.0×10^{-6} mg/mL with lower detection limit of 7.62×10^{-16} mg/mL. The developed procedure has been successfully used in assay of Cyt c in real samples.

1. INTRODUCTION

Recently, molecular imprinting(MIP) technology has received wide attention and has been extensively applied in the area of electrochemical sensors, which can create pre-designable materials for recognizing and quantifying specific target species [1]. Molecular imprinting bionic sensors can often supply a candidate to unstable biomolecules for industrial, medicine, and environmental analytical applications [2]. There have been a lot of molecular imprinting reports about detecting and separating small molecular compounds [2-9], but it is hardly applicable for complex biomacromolecules due to their particular properties [10]. Nowadays, surface imprinting techniques and electrochemical sensor can

be viewed as complementary technologies for generating protein imprinting electrochemical sensor, which can conquer the difficulties produced by large size and spatial structure complexity and effectively enhance sensitivity and selectivity of the resulting sensors. So far, the study on the protein molecular imprinting mainly focused on the adsorption and separation of proteins [11-13], relatively less on the protein analysis and sensing application. However, recently, more and more imprinting polymers have been employed for sensitive determination of the biomacromolecules by fluorescence [14, 15], especially electrochemistry, such as bovine hemoglobin (BHb) [16-19], human serum albumin (HAS) [20], bovine serum albumin (BSA) [21, 22], trypsin [23] and exhibited superior sensitivity and selectivity. There ever was a report that 10^{-16} mg/mL level of protein could be sensitively captured and detected by molecularly imprinting electrochemical sensor [24].

Cytochrome c is a typical water-soluble heme metalloprotein, which plays a pivotal role in electron transfer of the respiratory chain in the mitochondria. It is also one of the important tumor markers. So to develop sensitive, rapid and selective determination technique for cytochrome c is very necessary for diagnosing lung cancer disease [25].

Although direct electron transfer (DET) and electrochemical sensing of Cyt c have been widely reported[26, 27], their sensitivities are not high enough. It is a pity that the electrochemical imprinted biosensor of Cyt c for its fast recognition and quantitation is seldom seen so far.

Nanomaterials have drawn wide interest in the design of molecular imprinting sensors of protein because of their special performances including big effective surface area, strong adsorption ability, good catalytic efficiency and reaction activity [28], which can achieve large binding capacity of imprinted molecule as well as improve the electron transfer[29, 30]. Polyaniline (PANI) and multi-walled carbon nanotubes (MWCNTs) are extensively employed as ideal candidates for immobilizing protein owing to its outstanding biocompatibility, high conductive ability, big surface areas, cheapness, easy preparation, which can promote the protein DET and catalytic activity. By compositing of these materials, the resulting hybrid nanomaterials will combine their advantages and produce a synergy effect to achieve more excellent electrochemical properties.

In this work, a Cyt c molecular imprinting sensor was prepared for recognition and quantification of Cyt c by self-assembly of the nanomaterials and molecular imprinting polymer. We have designed an environment-friendly 3D nanostructure imprinted layer based on immobilization of Cyt c on the hybrid nanotubes composite. The imprinted sensor not only exhibited excellent recognition ability, but also reflected the intrinsic characteristics of the molecular imprinting. The prepared imprinted electrochemical biosensor demonstrated excellent reproducibility and stability as well as ultrahigh sensitivity and good selectivity for the determination of Cyt c.

2. EXPERIMENTAL

2.1. Chemicals

Cytochrome c (Cyt c, 95%), bovine hemoglobin (BHb, activity $\geq$ 20 KU/mg) and ovalbumin (OVA, 62 ~ 88%), horseradish peroxidase (HRP), bovine serum albumin (BSA, 98%) and lysozyme (Lys, activity $\geq$ 20 KU/mg) were used in experiments. Cyt *c* pharmaceutical injection was bought from

the local medicine store and the serum sample was supplied by a local hospital. Aniline, $(NH_4)_2S_2O_8$, H_2O_2 (30%) were of analytical grade and used without further purification. The multi-walled carbon nanotubes (MWCNTs, $\geq$ 95%) were further purified before use. Ultrapure water (Millipore, $\geq$ 18.2 MΩ cm) was used in whole experiment.

2.2 Apparatus

All electrochemical tests were carried out on a P4000 electrochemical workstation (Princeton, USA) with VersaStudio software. The three-electrode system was applied with bare or modified glassy carbon electrode (GCE, 3 mm in diameter) as the working electrode, Pt wire as the counter electrode and Ag/AgCl as the reference electrode. FT-IR spectra were measured on a Tensor II spectrometer using ATR(Bruke, German). UV-vis absorption spectra were recorded by a V757CRT UV-vis spectrophotometer (China). The morphologies and structures of the nanomaterials and a variety of modified electrodes were monitored by a Zeiss ULTRA Plus field emission scanning electron microscope (SEM) and a FEI TECNAL^2 F$_{20}$ STWIN D2278 transmission electron microscope (TEM).

2.3 Purification of MWCNTs

1.0 g MWCNTs were dispersed into the mixture of 10 mL HNO_3 (65%) and 30 mL H_2SO_4 (98%) in a 500 mL distilling flask equipped with condensation and exhaust gas absorption equipment. After ultrasonication for 20 min, the mixture was refluxed for 2h under magnetic stirring (the oil bath temperature gradually increased from 90 to 130 °C) to get the purified and carboxylated MWCNTs. The waste gas produced by the reaction was absorbed by NaOH solution. After cooled to room temperature, the sample was diluted with plenty of water and then vacuum filtered. The filter cake was washed repeatedly to neutral and filtered through a 0.22μm filter membrane and dried overnight at 50 °C in oven.

2.4 Preparation of nanotubular polyaniline (PANTs)

Nanotubular polyaniline were synthesized by a slightly modified reference procedure in the presence of excess oxidant ammonium persulfate [31,32]. The obtained product was named as PANTs.

2.5 Fabrication of the imprinted electrode (MIP/PANTs-MWCNTs) and the non-imprinted electrode (NIP/PANTs-MWCNTs)

glassy carbon electrode surface was pretreated using the reference method[32]. Before modification of nanomaterials, the bare electrode was inspected by cyclic voltammetry in 1.0 mM electrochemical active probe molecule solution until a pair of well-distinguished redox peaks occurred. The dispersion of nanomaterials was prepared by uniformly dispersing PANTs (2 mg) and MWCNTs (2 mg) into 4 mL ethanol under supersonic vibration. 9 μL (3.0 μL each time, 3 times) of the mixture solution was dropped on the surface of the treated electrode and it was left in the air to dry 60 min to

evaporate solvent. The PANTs-MWCNTs/GCE was obtained. Then, the composite material modified electrode was dipped in 1 mg/mL Cyt c solution prepared with pH 6.98 PBS buffer solution at least 48 h in a refrigerator at 4 °C. At last, the electrode was immersed in 25 mL of the PBS buffer containing 200 μL of aniline and cyclic-voltammetrically scanned for 5 cycles within - 0.2 to 0.8 V. Obtained electrode was called as Cyt c/PANTs-MWCNTs/GCE. To exclude the template Cyt c, Cyt c/PANTs-MWCNTs/GCE was dipped into 1.0 M HCl for 1 h under continuously stirring. The obtained MIP/PANTs-MWCNTs/GCE was completely re-washed with water. The removal of the Cyt c template was monitored by electrochemical methods. The imprinting electrode was kept in a refrigerator at 4 °C for further use.

At the same time, a non-imprinted NIP/ PANTs-MWCNTs/GCE was also fabricated in the same procedure without the template protein for comparison.

2.6 Electrochemical Analysis

Electrochemical characterization of the imprinted biosensor was performed with a three electrode cell. $K_3[Fe(CN)_6]/K_4[Fe(CN)_6]$ are selected as the probe molecules for monitoring the behavior of Cyt c considering the probe could penetrate into the molecularly imprinting film by formed imprinted cavities on the surface of the electrode.

CV scan was carried out in a 1.0 mM and 10.0 mM $Fe(CN)_6^{3-}$ solution with 0.1 M KCl as support electrolyte, respectively. The EIS was determined in 10.0 mM $Fe(CN)_6^{3-}/Fe(CN)_6^{4-}$ solution with 0.1 M KCl as support electrolyte, the frequency range was 100 mHz to 100 kHz and the amplitude was 5 mV. pH = 6.98 phosphate buffer was prepared from KH_2PO_4 and Na_2HPO_4 with 0.1 M KCl. Chronoamperometry was measured at different applied potential due to analyzed matter. The electrocatalytic determination was performed in high purity nitrogen saturated PBS solution for 20 min. BHb, BSA, OVA, HRP and Lyz were chosen for comparison to study the recognition capability of the proposed sensor. All tests were conducted at room temperature.

3. RESULTS AND DISCUSSION

3.1. Preparation and characterization of 3D nanostructure imprinted sensor

Three dimensional nanostructure was formed by modifying hybrid nanomaterials on the electrode surface. Protonated Cyt c (pH = 6.98, PI = 10.2) combined with carboxylated MWCNTs through electrostatic and π-π interactions, with PANTs through H-bond between C=O group of Cyt c and -NH$_2$ or -NH- groups to form imprinting sites. Scheme 1 shows the preparation process of the imprinted sensor.
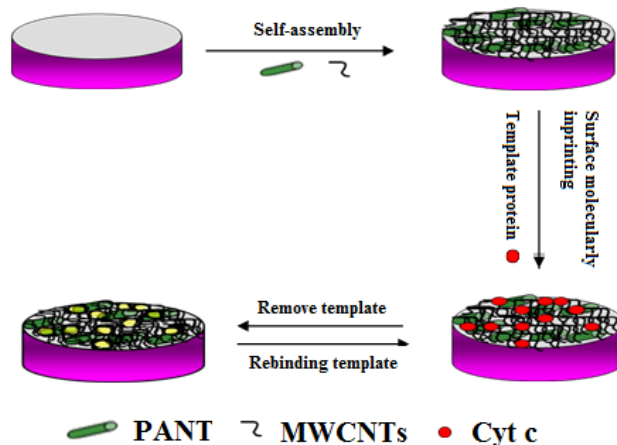
Scheme 1. The synthesis procedure of the MIP/PANTs-MWCNTs/GCE imprinting sensor

The large surface area of nanomaterials is beneficial to immobilize protein and provide an appropriate microenvironment to keep their bioactivity. MWCNTs can enhance electrocatalytic activity. Addition of PANTs further enhances the immobilized protein, and PANTs can effectively decrease the background current from MWCNTs too. When PANTs-MWCNTs were introduced onto GCE, the effective area evidently enhanced. As shown in Fig.1, the redox peak current response of PANTs-MWCNTs/GCE was much bigger than that of bare GCE (Fig. 1a and 1b). The effective surface areas of the bare GCE and PANTs-MWCNTs/GCE were 0.096 and 0.469 cm^2 respectively calculated by CV graph and Randles-Sevcik expression, where D is 0.76×10^{-5} cm$^2 \cdot$s^{-1} for Fe(CN)$_6^{3-}$ [33].
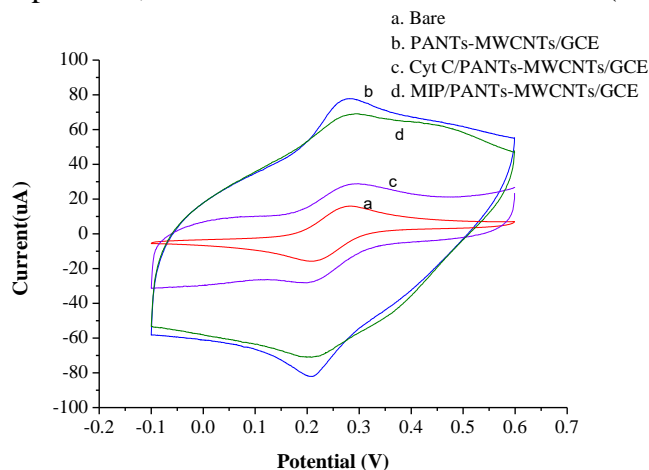

Figure 1. The cyclic voltammograms obtained at the modified electrodes in 1 mM Fe(CN)$_6^{3-}$ with 0.1 M KCl at the scan rate of 50 mV/s. (a) Bare GCE, (b) PANTs-MWCNTs modified GCE, (c) Cyt c/PANTs-MWCNTs/GCE before Cyt c removal, (d) MIP/PANTs-MWCNTs/GCE after Cyt c removal.

Cyt c template molecules can easily enter 3D nanostructure because of the interaction of these protein molecules with the nanotubes. When the protein protein was excluded from the 3D matrix, the

specific cavities for recognizing Cyt c molecules were formed. The template extraction from the 3D matrix could be detected by CV.

The redox current of the MIP/PANTs-MWCNTs/ GCE (Fig.1d) remarkably increased than Cyt c/PANTs-MWCNTs/GCE (Fig.1c). It was attributed to a formation of the imprinted sites after the template removal, which was advantageous to the electron transfer of the probes to the electrode surface by the cavities of the imprinted layer.
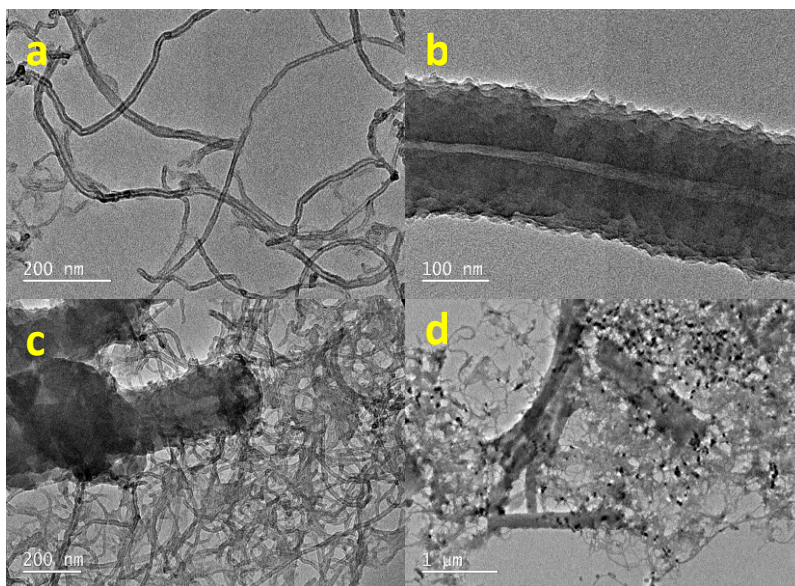
Figure 2. TEM images of (a) MWCNTs, (b) PANT, (c) PANTs-MWCNTs, (d) Cyt c-PANTs –MWCNTs

The shapes and structures of MWCNTs, PANTs, PANTs-MWCNTs and Cyt-PANTs-MWCNTs were displayed in Fig.2. The MWCNTs and PANTs showed uniform tubular and hollow shape, with average sizes of 14 nm and 180 nm, respectively, and the outer walls of PANI tubes looked very rough (Fig.2a, b and c). Fig. 2d shows Cyt c protein molecule was sphere-like particle with an mean size of 10 – 30 nm. in the meantime, the electrode surface was covered by a PANI thin film.

Fig. 3 displays the FESEM morphologies of the modified GCE and the imprinted layer. As seen in Fig.3a, bare GCE possessed a flat and smooth surface. Fig. 3b presents that MWCNTs compactly and uniformly dispersed and covered the surface of GCE. Fig. 3c shows the space stereo sense of PANTs modified GCE is stronger due to their much larger dimensions. When PANTs and MWCNTs were mixed and modified on GCE, a significant 3D network nanostructure in morphology was observed (Fig. 3d). Over 3D nanostructure, globular Cyt c protein molecules were easily immobilized on the surface of the hybrid nanomaterials, the resulting surface was more undulant (Fig.3e). It can be seen that there were lots of caves left after template molecule eluted in Fig.3f. The results showed that Cyt c molecules were successfully removed from the nanoarchitecture.
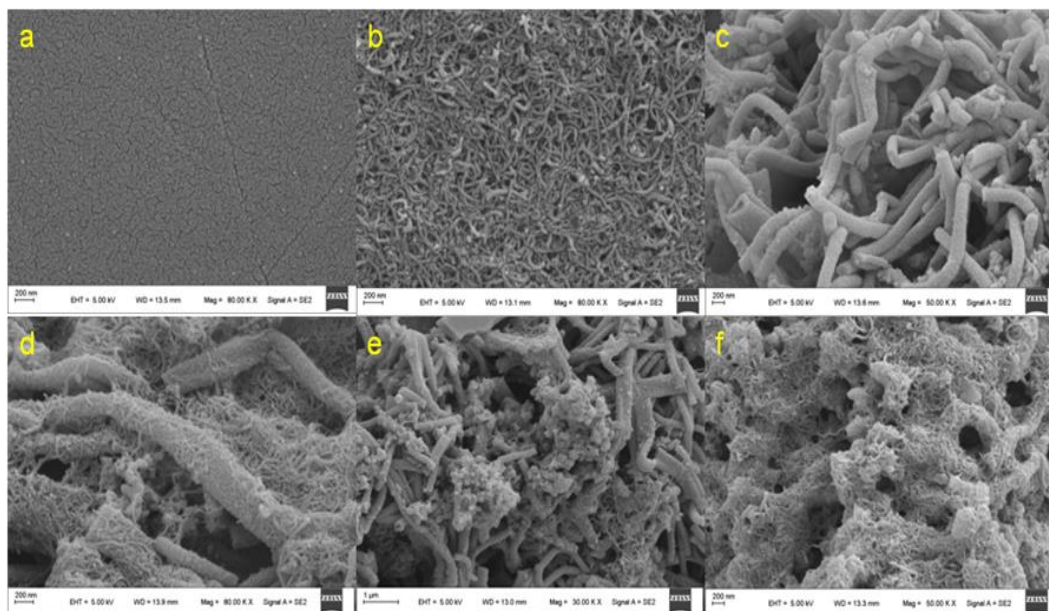
Figure 3. SEM images of different modified electrodes. (a) GCE, (b) MWCNTs/GCE, (c) PANTs/GCE, (d) PANTs-MWCNTs/GCE, (e) Cyt c/ PANTs-MWCNTs/GCE, (f) MIP/PANTs-MWCNTs/GCE.

UV-vis absorption spectroscopy was a helpful method to define whether protein still maintained its biological activity after the Cyt c interaction between with the nanometer materials [34]. On the other hand, this technique could also illustrate the effective disaggregation of MWCNTs because of the strongly absorption around 265 nm of individual nanotubes [35]. Fig.4 presented the UV-vis absorption spectra of the MWCNTs, PANTs, PANTs-MWCNTs, Cyt c and Cyt c-PANTs-MWCNTs. MWCNTs (Fig. 4a) had an obvious absorption peak at 256 nm owing to 1D van Hove singularities of single nanotube [36]. Fig. 4b illustrated the PANTs band at 264 nm. In Fig. 4d, original Cyt c possessed two characteristic absorption peaks at 409 nm and 530 nm (Soret and Q band, respectively) resulted from the porphyrin ring chromophore. Fig. 4e displayed the spectrum of Cyt c nanocomposite. The composite showed three bands, two of which were remarkable at 265 nm and 409 nm, but the Q band (530 nm) became weaker than native Cyt c. It suggested that the protein kept native and active. The 265 nm band was resulted from nanosize components because the addition of Cyt c made dispersion of nanotubes better [37].

MWCNTs, PANTs, Cyt c and Cyt c/PANTs-MWCNTs on GCEs were further characterized by FT-IR spectroscopy using ATR. MWCNTs/GCE showed characteristic absorption at 1736cm^{-1} and the O-H stretch vibrations at 2923 and 2849 cm^{-1}. PANTs/GCE displayed N-H bending vibration at 1581 cm^{-1}, C-C stretching vibration at 1151 cm^{-1} and C-C twisting vibration at 1244 cm^{-1}, respectively, as well as aromatic C=C stretching at 1495 cm^{-1}. At the same time, C-Cl stretching (695 cm^{-1}) and the other band (1043 cm^{-1}) which resulted from SO_4^{2-} produced by reduction of $S_2O_8^{2-}$ could be found too [38]. In IR spectra of Cyt c/GCE appeared the amide A N-H stretching at 3274 cm^{-1} and the amide II overtone vibration at 3066 cm^{-1} as well as astrong C=O vibration peak in amide II at 1642 cm^{-1}. At the same time, the band of 1531 cm^{-1} was assigned to the amide II N-H in-plane bending and corresponding C-N stretching. Adsorption of Cyt c on the hybrid nanomaterial surface would cause an obvious infrared absorption change related to native Cyt c, the characteristic peak of 1642 cm^{-1} has become weaker and

shifted to 1653 cm⁻¹. The peak at 1531cm⁻¹ almost disappeared. It explained that Cyt c had been successfully modified to the nanomaterials modified electrode surface.
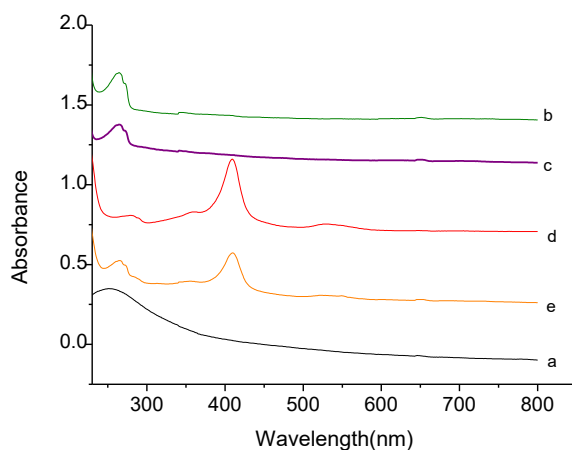

Figure 4. Optical absorption curves for (a) MWCNTs, (b) PANTs, (c) PANTs-MWCNTs, (d) Cyt c, (e) Cyt c-PANTs-MWCNTs in PBS (pH 6.98).

3.2 Electrochemical characteristics of Cyt c on the imprinting sensor

Adsorption of Cyt c on MIP/PANTs-MWCNTs/GCE was studied with incubation time varying from 3 to 300 min by the CV. The CV graphs of MIP/PANTs-MWCNTs/GCE were shown in Fig.5. When the imprinting sensor was dipped into Cyt c solution, the anodic and cathodic peak currents swiftly decreased, suggesting Cyt c molecules rapidly penetrating into the channels of the formed imprinting layer. In the first 20 minutes incubation, the peak currents dramatically declined. Then the peak currents started to rise. This is a process from disorderly to orderly, complying with the principle of self-assembly. Finally, the imprinted sensor gradually reached the adsorption equilibrium.
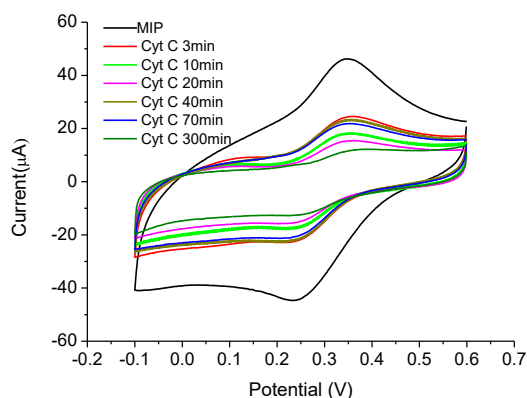

Figure 5. CVs of MIP/PANTs-MWCNTs/GCE incubated with Cyt c (1 mg/mL) different time in 1 mM Fe(CN)$_6^{3-}$.

3.3 Electrochemical sensitivity of the MIP/PANTs-MWCNTs/GCE toward Cyt c

Sensitive determination of the target is a key for MIP sensor. In this present study, the MIP/PANTs-MWCNTs/GCE was employed to measure Cyt c of different concentrations to estimate the sensitivity with CV method using 10 mM $Fe(CN)_6^{3-}/Fe(CN)_6^{4-}$ as redox probe in 0.1M KCl. Fig.6 showed that the redox peak current ΔI of on the MIP sensor decreased with Cyt c concentration increasing, which was because the template molecule entered imprinted cavities and blocked the the probe species diffusion through the imprinting layer. The peak current decrease was related with the Cyt c concentration. As depicted in the inset of Fig. 6, a good linearity for the cathodic peak current from 1.0×10^{-14} to 1.0×10^{-6} mg/mL was revealed and the linear regression equation was $\Delta I(\mu A) = -220.64 - 14.864 lgC_{Cyt\,c}$ ($R^2 = 0.9992$) and the detection limit (LOD) was 7.62×10^{-16} mg/mL (N =3), while for anodic peak current, the calibration plot gave a linear regression equation $\Delta I(\mu A) = 217.95 + 14.373 lgC_{Cyt\,c}$ ($R^2 = 0.9863$). It showed that reduction peak was more sensitive than oxidation peak for the detection of Cyt c. The low LOD mainly relied on the strong recognition performance of the imprinted sensor and the excellent biocompatibility of the hybrid nanomaterials.
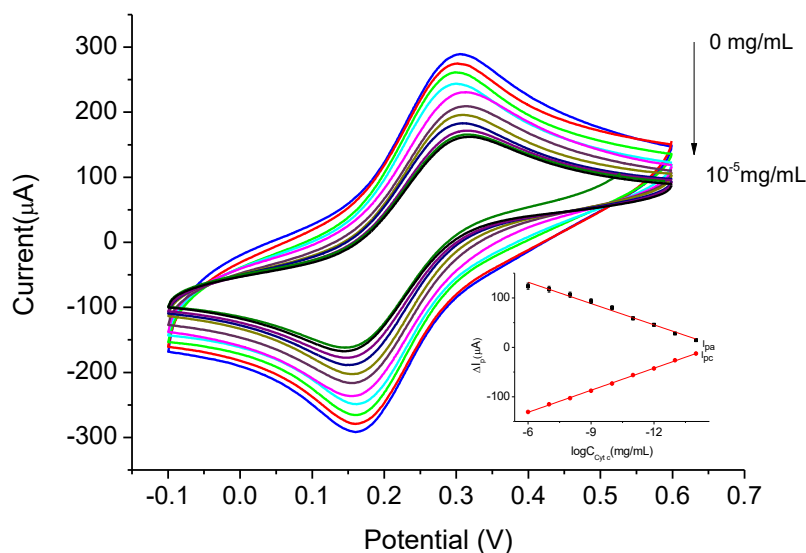

Figure 6. CV graphs of MIP/PANTs-MWCNTs/GCE in 10 mM $Fe(CN)_6^{3-}/Fe(CN)_6^{4-}$ for various concentrations of Cyt c for 5s (curves external to internal: blank, 1.0×10^{-14}, 1.0×10^{-13}, 1.0×10^{-12}, 1.0×10^{-11}, 1.0×10^{-10}, 1×10^{-9}, 1×10^{-8}, 1×10^{7}, 1×10^{-6}, 1×10^{-5} mg/mL), the inset was calibration plots of redox peak current versus concentration obtained from CVs data.

By contrast, the developed biosensor had a much higher sensitivity than the reported electrochemical sensors previously, such as gold nanoparticles modified polypyrrole grafted screen printed electrode (anti-cyt c/SAM/GNP/PPy/SPE, 2nM) [39] electropolymerized neutral red and decacarboxylated pillararene bearing terminal neutral red (NR) modified GCE (Poly-NR/ (P[5]A-COOH/GCE, 0.02~1.0nM) [40], cystamine, glutaraldehyde and PAMAM G4 dendrimers modified Au electrode (Cys/GA/PAMAM/Au, 5.0nM) [41], reduced GO-poly(amidoamine)/Au NPs modified

screen-printed electrode (ErGO/PAMAM-FAD/Au NPs/SPE, 1.0pM) [42], colloidal gold–dihexadecylphosphate stabilized MWCNTs composition film modified Au electrode (Au NPs–MWNTs–DHP/Au, 1.5μM) [43], 3D poly (orthanilic acid) nano-networks coated Pt electrode (POA/Pt, 5μM) [44], phthalocyanine stabilized Rh NPs modified GCE (Rh NPs capped with CoPTA/GCE, 33.3 nM) [45], Au NPs-doped bilayer lipid membrane composite modified GCE (Au/PC-LA/GC, 50nM) [46], single-strand DNA -functionalized Au NPs modified Au electrode (HS-ssDNA-Au NPs/Au, 0.67nM) [47], SWCNTs modified GCE (SWCNTs/GCE, 10.0μM) [48], Au NPs/three-dimensional silica gel network modified Au electrode (MSG/GNP/Au,8μM) [49], cytochrome oxidase/NiO-NPs/cMWCNT/PANI modified Au electrode (5pM) [50], fluorescence sensors, such as molecularly imprinted upconversion nanoparticles fluorescence sensor(UCNPs@MIP, 0.73 μM) [14], MIP-coated CdTe QDs fluorescence sensor (MIP-coated CdTe QDs, 0.41μM) [51] and N-doped graphene QDs/SiO$_2$/MIP fluorescence sensor (N-GQDs/SiO$_2$/MIP, 0.11μM)[15] and other sensing platform such as CPSPR aptasensor(50 pM) [52] , oriented surface epitope imprinted polymers-based QCM sensors (3.6 ng mL^{-1}) [53], neutravidin modified piezocrystalbased acoustic transducer (0.50 nM) [54] and so on. In addition, its linear range is also wider. A more detailed comparison of the sensor fabricated here and reported results was tabulated in Table 1.

3.4 Selectivity of the MIP sensor

Specific recognition was a crucial property of molecular imprinting. To further investigate selectivity of the sensor for Cyt c, BSA, OVA, BHb, HRP and Lyz were chosen as interfering species. The concentrations of the these proteins were all 0.1 mg/mL in PBS (pH = 6.98). The changes of the cathodic peak current (ΔI) on MIP/PANTs-MWCNTs/GCE and NIP/PANTs-MWCNTs/GCE in Fe(CN)$_6^{3-}$ with a series of proteins were measured by DPV mode. The selectivity was estimated by calculating ΔI$_{MIP}$. As shown in Fig.7, ΔI$_{MIP}$ toward Cyt c was the highest, which was respectively 2.29, 2.02, 2.42, 2.20 and 1.90 times of that for BSA, OVA, BHb, HRP and Lyz. At the same time, the imprint factor IF = ΔI$_{MIP}$/ΔI$_{NIP}$ for Cyt c was also the highest. These results obviously showed that the prepared imprinted sensor possessed better recognition ability for the Cyt c template molecule than other protein molecules. Compared with MIP/PANTs-MWCNTs/GCE, the non-imprinting electrode displayed lower recognition selectivity to Cyt c protein molecules. It is not difficult to understand that appropriate molecular dimensions of Cyt c made it easily access to the imprinted cavities. Furthermore, the interactions between the template and PANTs-MWCNTs provided strong binding force. Heme-protein with similar structure and molecular weight could also be adsorbed relatively easily to imprinted sensor. Besides, the current responses for Lyz on imprinting and non-imprinting electrodes were the relatively strong owing to its quite smaller molecular size, which would promote diffusion to the electrode surface and adsorption.

Table 1. Comparison of the prepared sensor with the previously reported results

| Sensor	Method	Linear range	LOD	Ref.
anti-cyt c/SAM/GNP/PPy/SPE	CV	2 nM -150mM	2 nM	39
Poly-NR/ (P[5]A-COOH/GCE	CV	0.2 nM – 5 μM	0.02 -1.0 nM	40
Cys/GA/PAMAM/Au	EIS, $K[Fe(CN)_6]^{3-/4-}$ as redox probe	0.1 nM–10μM.	5.0 nM	41
ErGO/PAMAM-FAD/Au NPs/SPE	DPV	2.5–320.0 pM	1.0 pM	42
Au NPs–MWNTs–DHP/Au	CV	1.5–45 μM.	1.5μM	43
POA/Pt	DPV	5μM - 70μM	5μM	44
CoPTA capped Rh NPs/GCE	DPV	100 nM - 3.0 μM	33.3 nM	45
Au/PC-LA/GC	SWV LSV	0.10 - 3.2 μM 0.40 -6.4 μ M	50nM 0.30μM.	46
HS-ssDNA-Au NPs/Au	CV	2nM – 0.10μM	0.67nM	47
SWCNTs/GCE	CV	30 - 700μ M	10μ M.	48
MSG/GNP/Au	CV	8- 120 μM	8μM	49
Cytochrome Oxidase/NiO-NPs/ cMWCNT/PANI/Au	Amperometry	5p M – 0.5μM.	5pM	50
UCNPs@MIP	Fluorescence	1-24μM	0.73 μM	14
MIP-coated CdTe QDs	Fluorescence	0.97μM-24μM	0.41μM	51
N-GQDs/SiO₂/MIP	Fluorescence	0.20-60 μM	0.11μM.	15
CPSPR aptasensor	SPR	80 nM –80 pM	50 pM	52
OEMIP-QCM sensor	QCM	$0.005\ \mu g\ mL^{-1}$ - $0.050\ \mu g\ mL^{-1}$	$3.6\ ng\ mL^{-1}$	53
Au/NA	Thickness shear mode acoustic method		0.50 nM	54
MIP/PANTs-MWCNTs/GCE	CV	1.0×10^{-8} - 1.0 ng mL^{-1}	7.62×10^{-10} ng mL^{-1}	This work
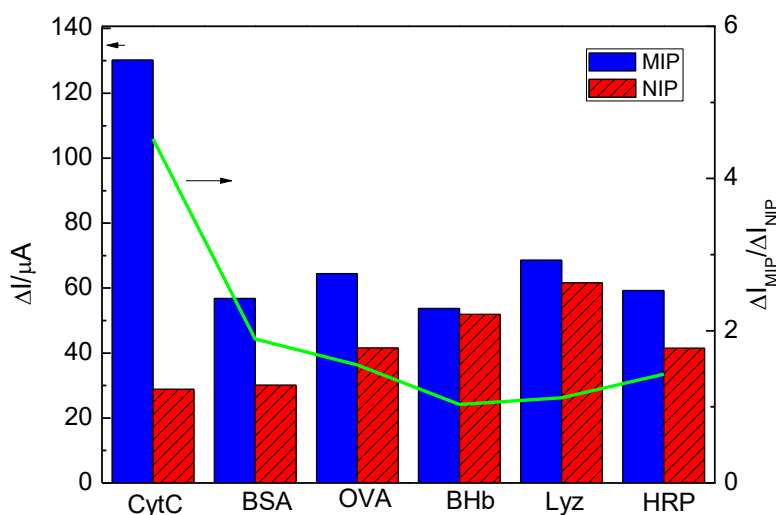
Figure 7. Selectivity of the MIP sensor in a 10 mM $Fe(CN)_6^{3-}$.

3.5 Repeatability, reproducibility and durability

The imprinted sensor displayed desirable repeatability, reproducibility and durability. The repeatability of the imprinting sensor was measured in 5.0 mM $Fe(CN)_6^{3-}$ solution by CV technique when the protein imprinting electrode was eluted with dilute acid. In the successive five measurements, the relative standard deviation (RSD) was only 2.14%. CV method was also employed to evaluate the reproducibility in 1 mM $Fe(CN)_6^{3-}/Fe(CN)_6^{4-}$ with five independently produced electrodes, which showed RSD was 5.24%. The long-term stability of the sensor was studied by monitoring the peak current in 5 mM $Fe(CN)_6^{3-}/Fe(CN)_6^{4-}$ by CV in 24 days maintained in 4 ℃. The peak current only declined 4% after 24 days compared with the initial value, indicating the protein imprinted sensor kept high stability. However, one point to note is that the 3D imprinted nanolayer may partially fall off if the molecular imprinted sensor is immersed in PBS solution for too long.

3.6 Real sample assay

The developed method was employed to determine Cytc in pharmaceutical injections. The injection was diluted with pH = 6.98 PBS buffer with 0.1 M KCl and then detected directly using the developed procedure through standard addition method. It was found that the recoveries were from 98.4% to 101.0%.

To determine the contents of Cyt C in serum sample, given amounts of the protein were spiked into 1.0 ml of serum samples. After mixed evenly, the spiked samples were diluted desired fold.

Analytical results were tabulated in Table 2, it was seen that for pharmaceutical injections, the recoveries were 98.4% to 101.0% while for serum sample, the recoveries were 98.8% to 103.1% and

RSD was less than 4%. The determined concentrations of Cyt c were also in agreement with the spiked ones.

Table 2. Analytical results of Cyt *c* in different real samples.

Sample	Added	Found	RSD%	Recovery%
Pharmaceutical	0	7.1	3.31	
injection	20	27.3	1.85	101.0
(mg mL^{-1})	50	56.4	2.50	98.6
	100	105.5	1.15	98.4
Human serum	0	4.9	0.91	
(µg mL^{-1})	20	25.2	0.72	101.5
	50	54.3	0.26	98.8
	100	108.0	2.09	103.1

4. CONCLUSIONS

By combining nanomaterials with self-assembly-surface molecularly imprinting technique, a novel and sensitive 3D structural electrochemical imprinted biosensor for Cyt c was prepared. The imprinted sensor delivered high selectivity, low detection limit as well as good durability for the template protein. Hence, the designed biosensor may supply a speedy and sensitive strategy for quantitative detection of Cyt c in the biological and medicine samples.

CONFLICTS OF INTEREST
There are no conflicts to declare.

References

1. L. Ye and K. Mosbach, *Chem. Mater.*, 20(2008) 859-868.
2. D. Kriz, O. Ramström and K. Mosbach, *Anal. Chem.*, 69(1997) 345 A-349A.
3. D. X. Nie, D. W. Jiang, D. Zhang, Y. Liang, Y. Xue, T. S. Zhou, L. T. Jin and G. Y. Shi, *Sens. Actuators* B, 156(2011)43–49.
4. C. G. Xie, H. F. Li, S. Q. Li, J. Wu and Z. P. Zhang, *Anal. Chem.*, 82(2010)241–249.
5. S. Noee, N. Salimraftar, M. Abdouss and G. Riazic, *Polym.Int.,* 62(2013)1711–1716.
6. M. Pesavento, G. D. Agostino, R. Biesuz, G. Alberti and A. Profumo, *Electroanalysis,* 24(2012) 813 – 824.
7. S. J. Li, Y. Ge, S. A. Piletsky and A. P. F. Turner, *Adv. Funct. Mater.*, 21(2011)3344–3349.
8. H. Y. Zong, X. Liu, Z. S. Liu and Y. P. Huang, *Electrophoresis,* 36(2015)818–824.
9. Z. H. Liu, Y. Yi, J. Gauczinski, H. P. Xu, M. Schonhoff and X. Zhang, *Langmuir,* 7(2011)11806–11812.

10. E. Verheyen, J. P. Schillemans, W. M. A. Demeniex van, W. E. Hennink and C. F. van Nostrum, *Biomaterials,* 32(2011) 3008-3020.
11. M. S. Zhang, J. R. Huang, P. Yu and X. Chen, *Talanta,* 81(2010)162–166.
12. E. Tamahkar, N. Bereli, R. Say and A. Denizli, *J. Sep. Sci.,* 34(2011) 3433–3440.
13. E. Tamahkar, T. Kutsal and A. Denizli, *Proc. Biochem.*, 50(2015)2289–2297.
14. T. Guo, Q. L. Deng, G. Z. Fang, C. C. Liu, X. Huang and S. Wang, *Biosens. Bioelectron.*, 74(2015) 498–503.
15. Y. J. Yan, X. W. He, W. Y. Li and Y. K. Zhang,*Biosens. Bioelectron.*, 91(2017) 253-261.
16. Z. H. Wang, F. Li, J. F. Xia, L. Xia, F. F. Zhang, S. Bi, G. Y. Shi, Y. Z. Xia, J. Q. Liu, Y. H. Li and L. H. Xia, *Biosen. Bioelectron.*, 61(2014)391-396.
17. J. Luo, S. S. Jiang and X. Y. Liu, *Sens. Actuators* B, 203(2014) 782-789..
18. S. Sun, L. Z. Chen, H. J. Shi, Y. J. Li and X. W. He, *J. Electroanal. Chem.*, 734(2014)18-24..
19. X. W. Kan, Z. L. Xing, A. H. Zhu, Z. Zhao, G. L. Xu, C. Li and H. Zhou, *Sens. Actuators* B, 168(2012)395– 401.
20. M. Cieplak, K. Szwabinska, M. Sosnowska, B. K. C. Chandra, P. Borowicz, K. Noworyta, F. D'Souza and W. Kutner, *Biosens. Bioelectron.*, 74(2015)960-966.
21. J. F. Xia, X. Y. Cao, Z. H. Wang, M. Yang, F. F. Zhang, B. Lu, F. Li, Y. H. Li and Y. Z. Xia, *Sens. Actuators* B, 225(2016)305-311.
22. M. X. Li, X. H. Wang, L. M. Zhang and X. P. Wei, *Anal. Biochem.*, 530(2017) 68-74.
23. G. Ertürk, M. Hedström and B. Mattiasson, *Biosens. Bioelectron.*, 86(2016)557–565.
24. D. D. Duan, H. Yang, Y. P. Ding, D. X. Ye, L. Li and G. H. Ma, *Electrochim. Acta*, 261(2018)160-166.
25. J. Javid, R. Mir, P. K. Julka, P. C. Ray and A. Saxena, *Tumor Biol.*, 36(2015) 4253–4260.
26. M. Pandiaraj, T. Madasamy, P. N. Gollavilli, M. Balamurugan, S. Kotamraju, V. K. Rao, K. Bhargava and C. Karunakaran, *Bioelectrochem.,* 91(2013) 1-7.
27. Y. Haldorai, S. K. Hwang, A. L. Gopalan, Y. S. Huh, Y. K. Han, W. Voit, G. SaiAnand and K. P. Lee, *Biosens. Bioelectron.*, 79(2016) 543-552.
28. I. Willner, B. Willner and E. Katz, *Bioelectrochem.,* 70(2007)2-11.
29. Y. Q. Lv, T. W. Tan and F. Svec, *Biotechnol. Adv.*, 31(2013)1172-1186.
30. S .Sun, L. Z. Chen, H. J. Shi, Y. J. Li and X. W. He, *J. Electroanal. Chem.*, 734(2014)18-24.
31. N. R. Chiou, J. Lee and A. J. Epstein, Chem. *Mater.*, 19(2007) 3589-3591.
32. Q. Wang, R. XUe, H. Guo, Y. L. Wei and W. Yang, *J. Electroanal. Chem.*, 734(2018)184-194
33. A. J. Bard and L.R. Faulkner, Electrochemical methods fundamentals and applications, 2nd ed, John Wiley & Sons,(2001)New York, USA
34. M. Eguílaz, A. Gutiérrez and G. Rivas, *Sens. Actuators* B, 225(2016) 74-80.
35. F. Lu, S, Zhang and L. J. Zheng, *Mol. Liq.,* 173(2012)42-46.
36. Y. H. Liu, L. Yu, S. H. Zhang, J. Yuan, L. J. Shi and L. Q. Zheng, *Colloids Surf.* A, 359 (2010)66-70.
37. K. Shanmugasundaram, G. Sai-Anand, A. L. Gopalan, H. G. Lee, H. K. Yeo, S. W. Kang and K. P. Lee, *Sens. Actuators* B, 228(2016)737-747.
38. N. Prabhaker, K. Arora, H. Singh and B. D. Malhotra, *J. Phys. Chem*. B, 112(2008)4808-4816.
39. M. Pandiaraj, N. K. Sethy, K. Bhargava, V. Kameswararao and C. Karunakaran, *Biosens. Bioelectron.,* 54(2014)115–121.
40. V. B. Stepanova, D. N. Shurpik, V. G. Evtugyn, I. I. Stoikov, G. A. Evtugyn, Y. N. Osin and T. Hianik, *Sens. Actuators* B, 225(2016)57–65.
41. A. Poturnayova, G. Castillo, V. Subjakova, M. Tatarko, M. Snejdarkova and T. Hianik, *Sens. Actuators* B, 238(2017)817–827
42. M. A. Tabrizi, M. Shamsipur, R. Saber and S. Sarkar, *Sens. Actuators* B, 240(2017) 1174–1181.
43. Y. H. Wu and S. S. Hu, *Colloids Surf.* B, 41(2005) 299–304.
44. L. Zhang, X. Jiang, L. Niu and S. J. Dong, *Biosens. Bioelectron.*, 21(2006) 1107–1115.

45. K. S. Lokesh, Y. Shivaraj, B. P. Dayananda and S. Chandra, *Bioelectrochem*., 75(2009) 104–109.
46. Y. Liu and W. Wei, *Anal. Sci*., 24(2008)1431-1436.
47. J. Zhao, X. L. Zhu, T. Li and G. X. Li, *Analyst,* 133(2008)1242–1245.
48. J. X. Wang, M. X. Li, Z. J. Shi, N. Q. Li and Z. N. Gu, *Anal. Chem*., 74 (2002) 1993-1997.
49. L .Wang and E. K. Wang, *Electrochem. Commun*., 6(2004) 49–54.
50. B. Batra, S. Lata, S. Rani and C. S. Pundir, *J. Biomed. Nanotechnol*., 9(2013)409-416.
51. W. Zhang, X. W. He, Y. Chen, W. Y. Li and Y. K. Zhang, *Biosens. Bioelectron*., 26(2011) 2553–2558.
52. F. C. Loo, S. P. Ng, C. M. L. Wu and S. K. Kong, *Sens. Actuators* B, 198(2014)416–423.
53. X. T. Ma,X. W. He,W. Y. Li and Y. K. Zhang, *Talanta,* 191(2019) 222-228.
54. P. Alexandra, C. Gabriela, S.Veronika, T. Marek, S. Maja and H. Tibor, *Sens. Actuators* B, 238(2017)817–827.